Joule

CellPress

Perspective

Neutron imaging of lithium batteries

Ralf F. Ziesche,[1,2,3,5] Nikolay Kardjilov,[4] Winfried Kockelmann,[5] Dan J.L. Brett,[1,2] and Paul R. Shearing[1,2,*]

SUMMARY

Advanced batteries are critical to achieving net zero and are proposed within decarbonization strategies for transport and grid-scale applications, alongside their ubiquitous application in consumer devices. Immense progress has been made in lithium battery technology in recent years, but significant challenges remain and new development strategies are required to improve performance, fully exploit power density capacities, utilize sustainable resources, and lower production costs. Suitable characterization techniques are crucial for understanding, *inter alia*, three-dimensional (3D) diffusion processes and formation of passivation layers or dendrites, which can lead to drastic capacity reduction and potentially to hazardous short circuiting. Studies of such phenomena typically utilize 2D or 3D imaging techniques, providing locally resolved information. 3D X-ray imaging is a widely used standard method, while time-lapse (4D) tomography is increasingly required for understanding the processes and transformations in an operational battery. Neutron imaging overcomes some of the limitations of X-ray tomography for battery studies. Notably, the high visibility of neutrons for light-Z elements, in particular hydrogen and lithium, enables the direct observation of lithium diffusion, electrolyte consumption, and gas formation in lithium batteries. Neutron imaging as a non-destructive analytical tool has been steadily growing in many disciplines as a result of improvements to neutron detectors and imaging facilities, providing increasingly higher spatial and temporal resolutions. Further, ongoing developments in diffraction imaging for mapping the structural and microstructural properties of battery components make the use of neutrons increasingly attractive. Here, we provide an overview of neutron imaging techniques, generally outlining advances and limitations for studies on batteries and reviewing imaging studies of lithium batteries. We conclude with an outlook on development methods in the field and discuss their potential and significance for future battery research.

INTRODUCTION

Batteries have attained a ubiquitous place in modern society, primarily through their application in consumer electronics. Advanced batteries will play a growing role in our lives and are a cornerstone of plans to achieve net zero, with ambitious aims to decarbonize transport and grid-scale energy storage. The primary constituent materials of lithium-ion batteries (LIB) were discovered in the 1970s and 1980s and commercialized in the 1990s. However, the maturation of the technology and the subsequent commoditization of these batteries has been a protracted, and indeed ongoing, process. Alongside the portfolio of batteries generally recognized

Context & scale

Increasingly demanding applications of batteries mandate an improved understanding of the performance, degradation, and failure of both materials and devices. Researchers have a portfolio of microscopy, spectroscopy, and diffraction tools to cover the increasing trend toward *multi-modal* and *in situ* or *operando* characterization, which provides an opportunity to probe the highly correlated physio-chemical phenomena associated with battery operation and degradation. Neutron imaging has made large strides in recent years to "catch up" with complementary X-ray imaging techniques and plays an essential role in device and materials characterization within the pantheon of battery analysis tools. Given the high sensitivity for lithium and the liquid electrolyte, neutron methods are especially suited for lithium battery studies. Further projected improvements to the suite of neutron techniques, with regard to spatial and temporal resolutions (largely enabled by hardware optimizations at current and planned neutron sources), will help tackle key contemporary challenges for current and next-generation battery chemistries.

as Li-ion, there is a growing interest in the development of revolutionary Li-ion and post Li-ion technologies; in the near term, these include low-cobalt cathodes and organic electrodes such as Li–S, Li–Si, or Li-air.[1] Limited resources and sporadic distributions of Li ore deposits stimulate the development of alternative charge carriers such as Na[2] or K[3], which are the focus of current research to compete with Li-ion technology. However, challenges remain with regard to structural transitions during cycling and associated structural instabilities resulting in lower capacity retention and a lower operational voltage. Batteries based on multivalent metals, such as Mg, Ca, Al, or Zn, have the potential for future large-scale energy storage based on the high abundance of the constituent materials in the earth's crust.[3] However, Na-/K-ions and multivalent ion alternatives alongside solid-state chemistries are currently at lower technology readiness levels. The diverse portfolio of possible applications for energy storage, which spans stationary and mobile applications from micro-Watt to mega-Watt scales, mandates a diverse collection of battery technologies. These variously balance key performance indicators, spanning energy and power density, cost, lifetime, safety, and recyclability.

To achieve the deployment of advanced battery technologies over short timescales, it is essential to accelerate their research and development. The development of new characterization tools is central to this goal, and the advances in *in situ* and *operando* monitoring capabilities with coupled modeling and simulation, provides a compelling opportunity to support the acceleration of these technologies.

Over the past decades, the development of imaging techniques has provided a unique insight into heterogeneous morphologies of battery electrode materials, alongside an improved understanding of device architectures. Magnetic resonance imaging (MRI) is sensitive to the nuclear magnetic resonance active nuclei, such as ^{1}H, ^{7}Li, or ^{23}Na,[4–6] and is able to provide quantitative information on chemical reactions,[7–9] transport processes in batteries,[10] and microstructure development such as Li or Na dendrite formation.[11,12] MRI provides a moderate spatial resolution of ≥ 10 μm and a small penetration depth into most metals of ≤ 10 μm. Electron microscopy (EM) offers significantly higher spatial resolutions, from the nanometer range of scanning electron microscopes (SEM) and transmission electron microscopes (TEM), to the sub-Å resolution of scanning transmission electron microscopes (STEM) for thin samples <300 nm.[13,14] A myriad of EM techniques and modalities enable a range of *in situ/operando* studies of solid electrolyte interphase (SEI) layers and dendrite formation,[15,16] liquid electrolytes in Li–S[17] and Li–Si[18] batteries, alongside other battery chemistries such as Zn.[19] X-ray imaging offers spatial and temporal resolutions ranging from sub-second failure events[20,21] to long term durability studies,[22] and from nanoscopic particle analysis[23] to testing of macroscopic devices.[24] Critically, X-ray tools have the penetrative power and tomographic capability to visualize processes of functional materials and working devices, such as cylindrical and pouch[20,25–28] cells. X-ray imaging applications cover a vast range of battery materials and chemistries. Alongside conventional absorption imaging, spectroscopic X-ray fluorescence computed tomography (XRF-CT) methods reveal the distribution of the constituent elements which can be correlated to results from other techniques such as transmission X-ray microscopy (TXM) and X-ray diffraction (XRD).[23]

Neutron imaging (NI) shares some important characteristics with X-rays and provides valuable, alternative contrast mechanisms. While X-rays are predominantly sensitive to electron density, neutrons are sensitive to nuclear density. Consequently, though some elements (e.g., lithium) are largely "invisible" to X-rays, they can be readily visualized using neutrons. Similarly, high-Z materials in construction or current

[1]Electrochemical Innovation Lab, Department of Chemical Engineering, UCL, London WC1E 7JE, UK

[2]The Faraday Institution, Quad One, Harwell Science and Innovation Campus, Didcot OX11 0RA, UK

[3]Diamond Light Source Ltd., Harwell Science and Innovation Campus, Didcot OX 11 0DE, UK

[4]Helmholtz-Zentrum Berlin für Materialien und Energie (HZB), Hahn-Meitner-Platz 1, 14109 Berlin, Germany

[5]STFC, Rutherford Appleton Laboratory, ISIS Facility, Harwell OX11 0QX, UK

*Correspondence: p.shearing@ucl.ac.uk

https://doi.org/10.1016/j.joule.2021.12.007

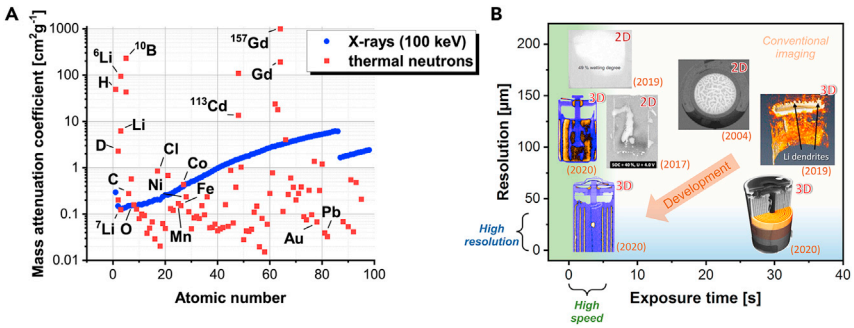

Figure 1. Comparison of the neutron and X-ray attenuation coefficient and development of NI techniques

(A) Mass attenuation coefficients for thermal neutrons (25 meV) and X-rays (100 keV). Attenuation is a combined process of absorption and scattering. The interaction of X-rays with the electron cloud gives rise to a near-monotonic increase in the attenuation coefficient, while the nuclear interaction of neutrons is not a regular function of the atomic number and also differs for isotopes of the same element.

(B) Spatial and time resolution development of NI for Li battery research over the last 20 years. The exposure times are given for a radiography (2D) or single projection of a computer tomography (3D) for corresponding spatial resolutions. Reprinted with permission from Song et al.[29] Copyright 2019 American Chemical Society. Reprinted from Ziesche et al.[30–32] CC BY 4.0. Reprinted from Goers et al.,[33] with permission from Elsevier. Reprinted from Starke et al.[34] CC BY NC ND 4.0. Reprinted by permission from Springer: Habedank et al.[35]

collection components in operating devices can overly attenuate an incident X-ray beam, leading to extended exposure times or low signal-to-noise ratios. Moreover, the isotopic sensitivity offered by neutron techniques enables enormous image contrast adaptability and dynamic investigation of materials evolution. NI, therefore, provides a helpful correlative tool to unravel the role of the myriad materials characteristic of operating battery devices.

The complementarity between neutrons and X-rays has been exploited for many decades; it is only more recently that substantial improvements in neutron flux and neutron detection have made NI (and indeed, tomography) a routine tool in the arsenal of scientific characterization techniques. Within fuel cell literature, the application of neutron radiography (NR) to visualize water is relatively widespread; however, the application of NI to battery investigations is somewhat more nascent.

From this perspective, we reflect on recent developments in NI characterization—which include significant progress in spatiotemporal resolution—and review its increasing role within battery research. With the growing portfolio of advanced batteries under development, and with a diverse material set spanning the periodic table, we identify a timely opportunity to explore the benefits and limitations of NI within the landscape of correlative imaging, diffraction, and spectroscopy tools. We use X-ray imaging as the point of reference for NI due to the abovementioned similarities and complementarity of the two probes.

Neutron radiography and tomography

Neutrons are chargeless particles and interact mainly with nuclei, in contrast to X-ray probes, which interact strongly with the charge of the electron shells of atoms. Therefore, neutron beam attenuation does not depend on the atomic number, while for X-rays, the high-Z elements are stronger absorbers than low-Z elements. The smaller size of the nucleus compared with the electron shell is the reason neutrons

are absorbed only weakly by many common materials. Hence, imaging with neutrons allows for the penetration of thick layers of metals, while providing high sensitivity to some light elements, even if these are embedded in a closed metallic environment. Figure 1A illustrates the mass attenuation coefficients of neutrons of the elements compared with 100 keV X-rays. Neutron interactions vary randomly across the periodic table and may differ drastically for isotopes of the same element.

In the following discussion, we refer to radiography as the process of producing a radiogram or 2D projection of an object, and we refer to tomography (N-CT) as the process of producing a 3D real-space presentation from which cross-sectional slices can be extracted. We use the higher-level term NI to refer to NR and N-CT, as well as to spatially resolved diffraction.

Conventional neutron attenuation radiography is based on the transmission of a collimated beam of thermal (wavelengths: ca. 1.0–2.5 Å) or cold neutrons (>2.5 Å) through a sample, and the recording of the attenuated beam by a position-sensitive detector.[36,37] The transmitted intensity obeys Lambert-Beer's law, stating that for a given neutron energy, the ratio of the transmitted and the incident intensity is an exponential function of thickness multiplied by the attenuation coefficient of the sample.

For tomographic imaging, the sample is rotated in the beam stepwise around a fixed (mostly vertical) axis, allowing for the acquisition of a projection image at each rotation angle using a position-sensitive detector. The recorded set of angular projections is subjected to filtering and flat-field correction operations and is then used for tomographic reconstruction. In this way, the entire volume of a sample can be unraveled in 3D by reconstructing the attenuation coefficient for each voxel of a sample from the collected projections, using mathematical algorithms such as filtered back projection or noise-suppressing iterative algorithms.[36,38] The spatial resolution of NI typically ranges between 5 and 200 μm, but can range up to millimeters for diffraction imaging.

Attenuation coefficients vary with neutron wavelength, which needs to be taken into account when interpreting grayscales and attenuation levels in terms of materials compositions. Moreover, crystal monochromators and time-of-flight methods are used for wavelength-selection at reactor sources and accelerator-based pulsed spallation sources, respectively. By distinguishing neutron wavelengths, details of the two most important attenuation mechanisms in NI can be exploited: neutron absorption and neutron (Bragg) diffraction.[39] For Bragg-edge imaging, every camera pixel measures a spectrum rather than a grayvalue. Bragg edges are sudden jumps in the neutron transmission due to neutrons being removed by Bragg-diffraction. By analyzing positions, widths, and heights of Bragg edges, one can map structural properties and crystallographic phases in 2D and 3D, albeit with coarse spatial resolutions of a few hundred microns. Furthermore, isotopes and elements can be mapped using neutron resonances at pulsed sources.[40] These transmission methods are complemented by spatially resolved neutron diffraction with a pencil-beam and by recording the scattered neutrons; this method provides rather coarse (mm[41]-sized spatial resolution[42]), but nonetheless exquisite information about structural and microstructural details in each voxel, such as internal strains and grain orientation. It is worth noting that further advanced NI methods are being developed,[37,43] but have not yet been used for battery studies. Phase contrast imaging exploits refraction of neutrons at interfaces to enhance the contrast between features that are indistinguishable via attenuation. Dark-field imaging[44] is capable of characterizing

nano- and microstructural properties, such as pore sizes and particle shapes, with a spatial resolution of a few hundred microns. Imaging with polarized neutrons[45] usually exploits the neutron interaction with magnetic moments in materials and can potentially be used to distinguish incoherent hydrogen scattering from other interaction types.

Advantages/limitations of neutrons for Li-ion batteries

The sizes of the battery components, such as electrodes, separators, and solid electrolytes, are in the micrometer range. Further, the dynamics of Li-ion diffusion processes during battery operation are monitored in the time range of minutes. These boundary conditions have initiated a tremendous improvement in both spatial and time resolution of NI in recent years, see Figure 1B. The additional demand for non-invasive *in situ* and *operando* investigations became an important catalyst for the extension to 4D (3D spatial and time) imaging capabilities. This allowed for dynamic volumetric studies of the distribution and movement of light elements, such as lithium and hydrogen, in material components and in complete devices that are used for energy conversion and storage, such as fuel cells and batteries.

Li batteries are suitable objects for NI because neutrons have a high visibility for Li-ion charge carriers and hydrogen-containing electrolytes, which is required to visualize migration of Li-ions and subsequently to identify areas of reduced activity that are responsible for capacity decline. During dis-/charge, a dynamic 3D measurement of the change in Li concentration can be performed by measuring the change of neutron attenuation coefficients in corresponding areas of the battery volume. Moreover, as mentioned above, neutrons interact with the nuclei of atoms and are, therefore, sensitive to isotopes rather than elements, for example, of lithium or hydrogen, which allows for the application of isotopic labeling. Compared with highly attenuating ^{1}H and ^{6}Li, the neutron beam attenuation for ^{2}H (D) and ^{7}Li is relatively low. This can be used to enhance the visibility of hydrogen or lithium in particular battery components, and not in others. Thus, Li exchange processes inside batteries can be followed by using, for example, ^{6}Li on the anode side and ^{7}Li or ^{nat}Li on the electrolyte or cathode side, to provide important information about the dynamic properties of the lithium diffusion during battery dis-/charging.

Neutrons and X-rays effectively complement each other in many cases, with regard to visibility of and access to material features, components, and physical properties. Nevertheless, neutrons fluxes are low and, by nature of the weak interaction, neutrons are more difficult to detect, leading to comparatively low counts in image camera pixels, and/or to much longer exposure times for the same grayvalues. The achievable spatial and temporal resolutions are limited, and images are much more affected by low signal-to-noise compared with X-ray CT studies. This is why broad-band ("white") neutron beams are employed without energy-discrimination where possible, even though some information is averaged out (e.g., Bragg edges) and even if white-beam imaging introduces additional difficulties with the analysis of the neutron images. For high-absorption elements such as Li, for example, the measured attenuation coefficients depend strongly on the wavelength band used, and beam-hardening artifacts necessitate extra corrections of the neutron images. It is furthermore worth noting that, as a downside of the abovementioned high sensitivity for hydrogen, parasitic scattering of neutrons into the camera screen produces scattering artifacts and hampers quantification of the material properties.

Neutrons produce no radiation damage in battery devices, while beam damage in X-ray synchrotron applications is sometimes problematic. On the other hand,

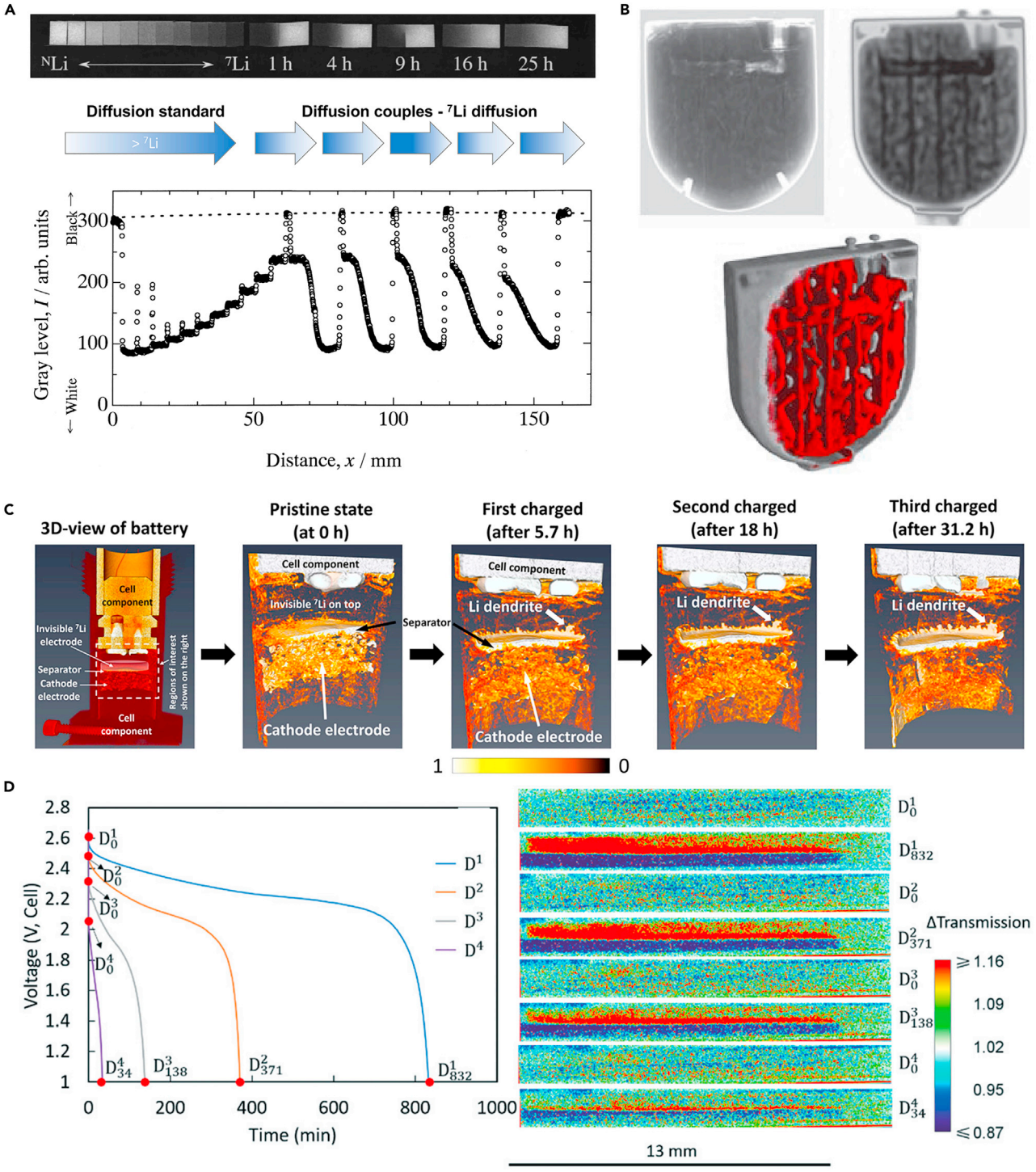

Figure 2. Lithium diffusion studies using NR and N-CT

(A) NR study on standard samples with varying ^{7}Li contents and on diffusion couples of $Li_{1.33}Ti_{1.67}O_4$ (top) and corresponding digitized intensity spectra (bottom). Reprinted from Takai et al.,[48] with permission from Elsevier.

(B) X-ray (top left) and neutron (top right) radiographs of a lithium-iodine cell after discharging, and rendered lithium distribution from an N-CT scan (bottom). Republished with permission from IOP Publishing, from Strobl et al.,[51] permission conveyed through Copyright Clearance Center.

(C) N-CT of dynamic dendrite growth by Song et al.[29] indicating the dendrite evolution in a $^{7}Li/LiMn_2O_4$ electrochemical half-cell at several stages of charge and the disappearance after discharge with transparent ^{7}Li-anode. The color bar represents increased neutron absorption from 0 to 1. Reprinted with permission from Song et al.[29] Copyright 2019 American Chemical Society.

Figure 2. *Continued*
(D) Time-lapse NR of thick sintered $Li_{4+y}Ti_5O_{12}/LiCoO_2$ electrodes discharged at C/20 (blue), C/10 (orange), C/5 (gray), and C/2.5 (purple), with the discharge profiles on the left and corresponding radiographs on the right. Red pixels indicate regions of lower lithium concentrations in the $Li_{4+y}Ti_5O_{12}$ electrode; blue pixels indicate lithium accumulation in the $LiCoO_2$ electrode. Republished with permission of the Royal Society of Chemistry, from Nie et al.[52]; permission conveyed through Copyright Clearance Center.

neutron-induced sample activation cannot be avoided and may pose logistical challenges if battery cells are to be studied by other methods immediately following the neutron analysis. However, the activation is usually short-lived and decays in a matter of days.

Neutron imaging on Li batteries—a review of recent work

While the advantages of NI over X-rays for lithium transport studies are often emphasized, the volume of applications of NR and N-CT on LIBs is remarkably small, most likely related to the over-powering absorption of lithium and related problems with opaque neutron images, moderate spatial resolution, sample activation, and lack of neutron source strength for time-lapse studies. There are three main lines of investigations: lithium diffusion, electrolyte consumption with associated gas evolution, and filling of cells with electrolytes. A small number of studies were concerned with the evolution of structures and microstructures during dis-/charging and lithium de-/intercalation by neutron diffraction and Bragg-edge imaging. Beyond that, N-CT was used to confirm, post-mortem, the absence of exterior lithium salt depositions on a Boeing 787 "Dreamliner" lithium battery, supporting the assumption of an internal short.[46]

NI experiments on Li-ion electrodes and battery cells date back to the 1990s, with the first lithium diffusion studies by Kamata et al.[47] using NR to visualize the Li-ion movement between two spinel-type $Li_{1.33}Ti_{1.67}O_4$ electrodes, prepared with the less absorbing ^7Li isotope and with a natural $^7Li/^6Li$ mixture used as cathode and anode, respectively. Likewise, Takai et al.[48,49] measured lithium diffusion coefficients in $Li_{1.33}Ti_{1.67}O_4$ and $La_{2/3-x}Li_{3x}TiO_3$ using different lithium isotope concentrations, see Figure 2A. The first investigations on lithium distributions in primary and secondary commercial battery cells, for charged and discharged states under different dis-/charge conditions, were performed by Kamata et al.[50]

The development of digital NI camera systems using charged coupled devices (CCD), CMOS sensors, or microchannel plates (MCP) enabled tomographic scans and *in situ* NR and N-CT analyses during cycling of lithium cells. Kardjilov et al.[53] produced an N-CT scan of a lithium-iodine battery cell of a pacemaker device providing lithium distributions before and after cycling, as shown in Figure 2B. Further, Song et al.[29] showed that time-resolved NR can contribute to studies of the dynamic redistribution processes related to dendrite growth from lithium plating and stripping, which can cause short circuits in lithium-metal batteries. In the study they used a ^7Li-anode|separator|$LiMn_2O_4$-cathode ensemble with a thick cathode configuration to study the dendrite formation. The large dendrites were clearly visible with the available spatial resolution of the NI system (Figure 2C). The cell was charged several times and finally discharged whereby *in operando* radiographs were taken and N-CT data collected at the end of each cycle step. The N-CT data clearly showed the separator and the natural lithium cathode particles below the separator. Due to its lower neutron cross-section, the ^7Li anode appears transparent. The results demonstrated the growth of dendrites at each charge step and loss of dendritic structure following discharge. Beside the low attenuating ^7Li isotope, high absorbing ^6Li helps to improve the visibility of fine changes in Li concentrations in small electrode samples, such as demonstrated by Wang et al.,[54] who studied Li distribution during ^6Li

intercalation in highly oriented pyrolytic graphite (HOPG). With time-resolved NR, they found a highly non-uniform Li distribution during the lithiation process with spots of large Li concentrations.

Tomographic NI has historically been limited by long collection times in the range of hours. NR, on the other hand, allows for *in situ* or *operando* analysis of lithium transport in parallel aligned electrode configurations, for which path integrals along the neutron trajectory are meaningful and with collection times in the range of seconds. High spatial resolution is required to achieve reasonable data on thin tailored electrodes that enable high dis-/charge currents with short Li-ion paths between electrodes of commercial Li-ion cells. Siegel et al.[55,56] performed high resolution (20 μm) NR to investigate lithium transport in $LiFePO_4$/graphite pouch cells with electrode thicknesses between 40 and 100 μm. The setup enabled the detection of dynamic lithium concentrations, spatially resolved across the electrodes at different states of charge (SoC), and allowed the authors to follow the electrode swelling/thickness changes during lithium de-/intercalation. A sub-pixel resolution method revealed an irreversible electrode expansion as a result of high C-rate charging and non-uniform lithium staging. Other studies have used thick electrode configurations to circumvent the coarse resolution of NI: Owejan et al.[57] took advantage of a 300-μm-thick graphite composite electrode to quantify the lithium intercalation and study capacity loss in relation to trapped lithium. Zhou et al.[58] utilized a 700-μm-thick lithium-metal electrode sandwiched between two bulky graphite electrodes to demonstrate a gradual change of neutron transmission. Nie et al.[52,59] applied NR on sintered $Li_{4+y}Ti_5O_{12}$/$LiCoO_2$ full cells with electrodes up to, and thicker than, 600 μm in a coin cell configuration. By cycling with different current densities, more lithium was transported at lower currents, resulting in higher capacity, and Li-ion de-/intercalation only occurred close to the separator for high C-rates, such as shown in Figure 2D. The same study showed that electrode tortuosity had only a small influence at low C-rates.

N-CT is the preferred technique to unravel lithium diffusion inside spiral-wound battery cell designs. However, additional challenges have to be met to characterize such batteries, due to the high neutron-attenuating elements in the active electrode materials, such as Ni, Mn, or Co, in addition to Li. CT reconstructions of large LIBs using polychromatic neutrons show significant reconstruction artifacts such as beam hardening, as demonstrated by several authors.[60–63] Such artifacts can be either prevented by using a monochromatic neutron beam,[62]—which, however, increases exposure times severely—or by applying a beam-hardening correction during CT reconstruction. Generally, the low neutron transmission through cells and the related low counting statistics often limits investigations to *ex situ* studies.

Zhang et al.[64] demonstrated that N-CT is well suited to study the 3D lithium distributions in the de-/lithiation SoC of <1 mm thick V_2O_5 cathodes of commercial coin cells. The charged and discharged cells displayed different Li distributions, with a higher non-uniformity observed for the higher C-rate cycled electrodes. Further, Nanda et al.[65] visualized the variation of the discharge products across the bulk of the electrode in 3D to support a kinetically coupled diffusion-based transport model for lithium-air batteries.

Strobl et al.[51] exploited the complementary imaging contrast for neutrons and X-rays for a lithium-iodine battery cell (Figure 2B). *In operando* X-ray and NR was used by Sun et al.[66] to study the lithium alloying of Si-particles, demonstrating the particle evolution during the first discharge, by taking advantage of increasing transmission for X-rays and decreasing transmission for neutrons. Longer exposure times for

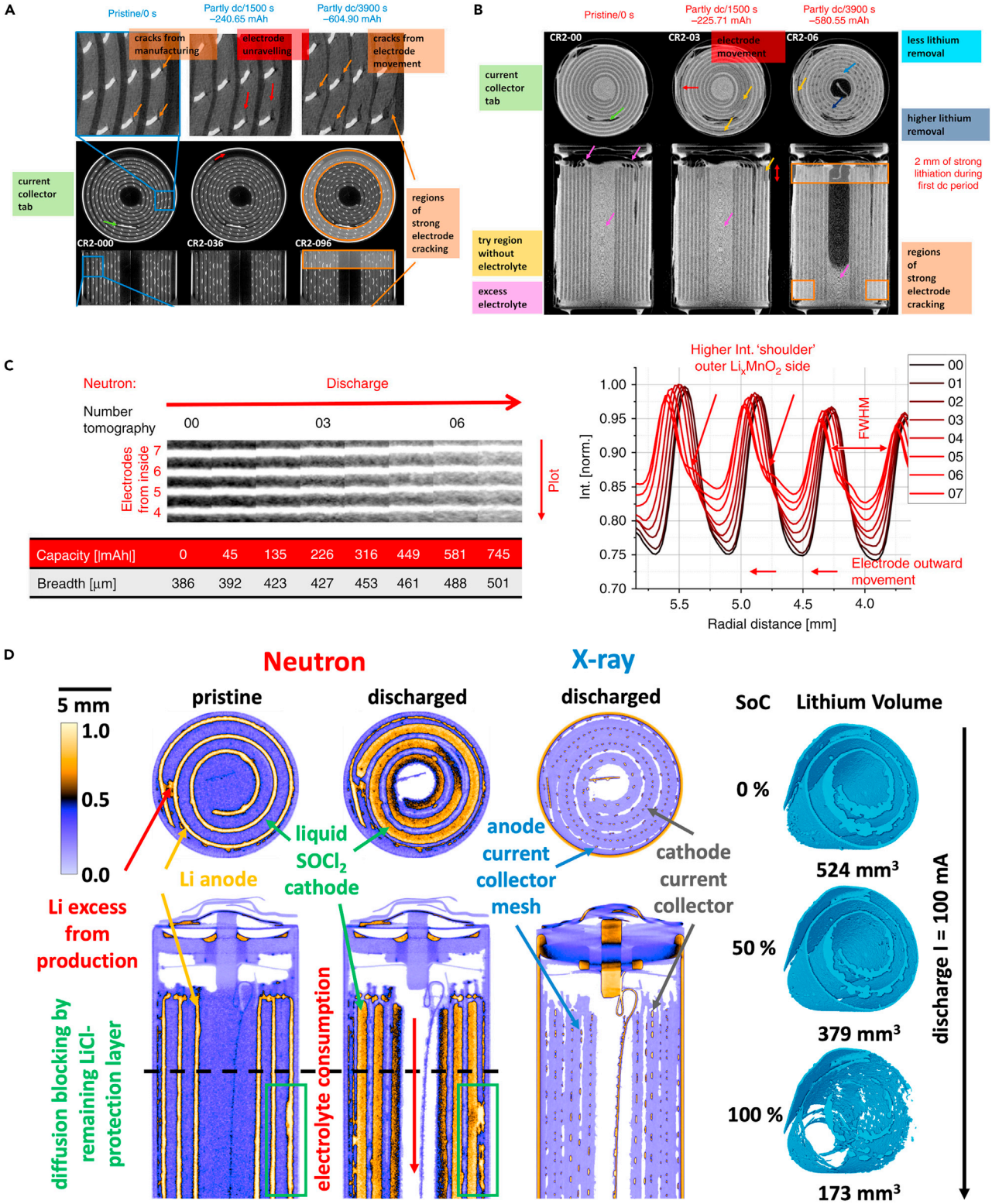
A
Pristine/0 s
Partly dc/1500 s
−240.65 mAh
Partly dc/3900 s
−604.90 mAh
cracks from manufacturing
electrode unravelling
cracks from electrode movement
current collector tab
regions of strong electrode cracking
CR2-000
CR2-036
CR2-096
B
Pristine/0 s
Partly dc/1500 s
−225.71 mAh
Partly dc/3900 s
−580.55 mAh
CR2-00
CR2-03
CR2-06
electrode movement
less lithium removal
higher lithium removal
2 mm of strong lithiation during first dc period
current collector tab
try region without electrolyte
excess electrolyte
regions of strong electrode cracking
C
Neutron:
Discharge
Number tomography
00
03
06
Electrodes from inside
7
6
5
4
Plot
Capacity [mAh] 0 45 135 226 316 449 581 745
Breadth [µm] 386 392 423 427 453 461 488 501
Higher Int. 'shoulder' outer LixMnO2 side
Int. [norm.]
1.00
0.95
0.90
0.85
0.80
0.75
0.70
FWHM
00
01
02
03
04
05
06
07
Electrode outward movement
5.5
5.0
4.5
4.0
Radial distance [mm]
D
Neutron
X-ray
5 mm
1.0
0.5
0.0
pristine
discharged
discharged
SoC
Lithium Volume
0 %
524 mm³
liquid SOCl2 cathode
anode current collector mesh
cathode current collector
Li anode
Li excess from production
50 %
379 mm³
diffusion blocking by remaining LiCl-protection layer
electrolyte consumption
100 %
173 mm³
discharge I = 100 mA

Figure 3. 4D time resolved neutron and X-ray CT imaging

(A and B) 3D reconstructed orthogonal slices of *in operando* X-ray CT (A) and N-CT (B) of a CR2 Li/MnO_2 cell during discharging over a 4.5 and a 4.7 Ω resistor.

(C) Shows cut-outs of the virtual unrolled multilayer sections at different SoC displaying the grayvalue changes, volume expansion of the MnO_2 electrode, and electrode movement as a result of the lithium migration. Reprinted from Ziesche et al.[30] CC BY 4.0.

(D) Lithium mass transport from the lithium-metal anode to the liquid thionyl chloride cathode of a Li/$SOCl_2$ ER14505M cell discharged with 100 mA as orthogonal slices from 4D N-CT and post-mortem X-ray CT data, alongside the quantified lithium anode depletion. Reprinted from Ziesche et al.[31].

high resolution N-CT often reduces the applicability of the complementary imaging techniques to post-mortem studies, as shown by Sun et al.[67] in their investigation of structural changes in cycled lithium-oxygen batteries. Nonetheless, the work by La-Manna et al.[68,69] provided further evidence for the useful complementarity of X-ray and N-CT for the inspection of commercial LIBs where, *inter alia*, neutrons identify the lithium-containing components and the electrolyte, and X-rays highlight metallic components such as the electrode current collectors and cabling in a battery cell.

The successful combination of both tomographic techniques on commercial lithium batteries was demonstrated by Ziesche et al.[30] using *in operando* X-ray and *in situ* N-CT on commercial CR2 Li/MnO_2 cells. The X-ray CT data revealed structural changes, such as electrode cracking, particle movement, and volume expansion due to lithium intercalation in the MnO_2 cathode shown in Figure 3A. Conversely, N-CT tracked the electrochemistry such as the lithium removal from the lithium-metal anode, the electrolyte consumption and inactive regions where electrolyte and/or lithium are fully consumed such as shown in Figure 3B. In combination with a novel virtual unrolling tool, both techniques revealed subtle changes through and along the electrodes which are normally "obscured" in the spirally wound electrode structure. Figure 3C demonstrates the unrolling method used to follow the lithium transport, electrode movement, and expansion of multilayer sections of the measured N-CT datasets at different SoC. Further, Ziesche et al.[31,32] demonstrate first 4D (3D spatial and 1D time resolved) N-CT experiments on commercial Li/$SOCl_2$ battery cells with complementary X-ray CT in a two-part study using different NI instruments. With appropriate CT scanning strategies for neutrons,[70] such as the golden-ratio[71] scheme, the authors provide a quantitative correlation between the lithium that is removed from the lithium-metal anode with the discharge current and the electrolyte consumption. Figure 3D illustrates the pristine and the discharged SoC of an ER14505M cell scanned with an on-the-fly scanning strategy and a post-mortem X-ray CT that displays the anode and cathode current collectors that are less visible with neutrons. The complementary X-ray CT helped do identify *inter alia* the LiCl protection layer on the anode surface and the nickel current collector meshes inside both electrodes, which are invisible to neutrons because these parts exhibited similar attenuation coefficients to the surrounding components.

NI is well suited to study electrolyte consumption and resulting gas evolution from electrolyte decay, as well as formation of the SEI in lithium cells. This is due to the high sensitivity of neutrons for hydrogen. A number of NR studies describe an irreversible consumption of excess electrolytes during the first cell charge accompanied by gas evolution. Lanz et al.[72] utilized NR to study the gas evolution and the resulting displacements in commercial prismatic Li-ion cells during the first charge-discharge step, concluding that most of the gas formation happened in the first charge period. Goers et al.[33] used NR to compare different PVDF-based gel-type electrolytes by their percentage levels of evolved gas on the graphite electrode. Figure 4A presents four of the *in situ* radiographs taken during the first charge step with an EC:PC 2:3 1M $LiClO_4$ electrolyte mixture. The increased production of bubbles and channels indicated gas evolution, which correlated well with the electrochemical data. Furthermore, the process of gas formation in high voltage Li-ion pouch cells was

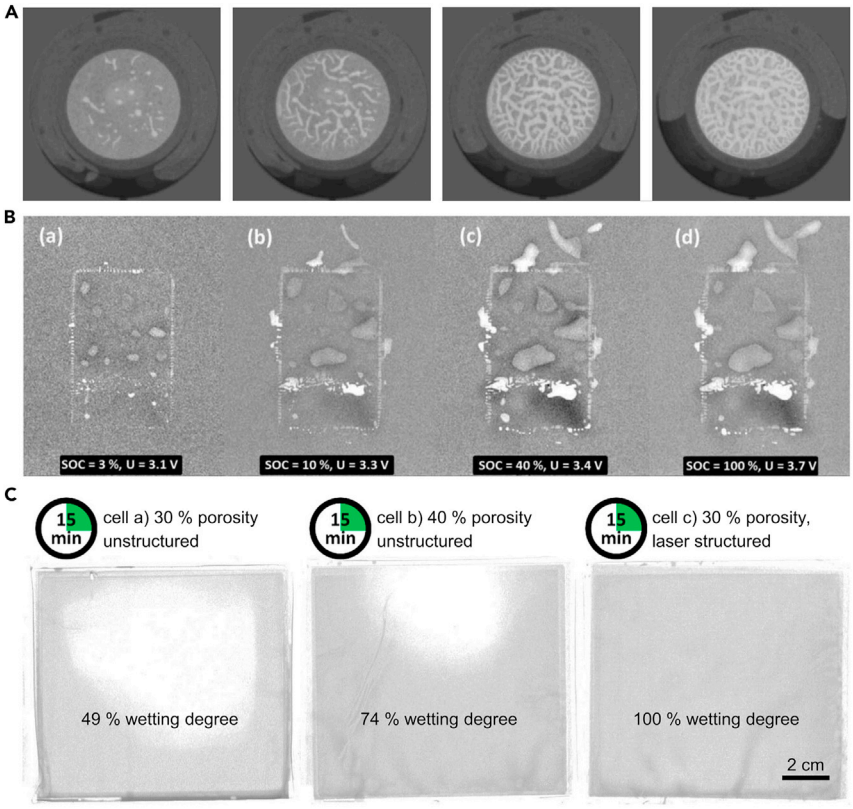

Figure 4. Visualization of the gas evolution and electrolyte wetting using NR

(A) Normalized radiographs visualize the gas evolution (from left to right) in a graphite/$LiMn_2O_4$ cell with EC:PC 2:3 1M $LiClO_4$ electrolyte mixture during the first charge. Reprinted from Goers et al.,[33] with permission from Elsevier.

(B) Radiographs of $LiFePO_4$/graphite (a)–(d) at different SoC and cell potentials normalized to the initial radiograph. Reprinted from Starke et al.[34] CC BY-NC-ND 4.0. The electrolyte displacement by evolved gas is visible as large bright areas where the intensity correlates to the amount of gas.

(C) *In situ* NR of the electrolyte wetting of multilayer pouch cells with different porosity and laser structured electrodes. A higher electrode porosity indicates faster cell wetting, whereby laser structured electrodes show a significant increase in cell wetting after filling with electrolytes. Reprinted by permission from Springer: Habedank et al.[35]

investigated qualitatively and quantitatively by Michalak et al.[73,74] and Starke et al.[34] The gas evolution was based on oxidation and reduction of electrolyte solvents separated for anode and cathode. The use of NR alongside differential electrochemical mass spectroscopy (DEMS) or prompt gamma activation analysis (PGAA) allowed the gas species to be determined: C_2H_4 and H_2 formed on the graphite anode, and CO_2 formed on the cathode. *In situ* and *operando* NR mapped regions of high activity following the charging process (Figure 4B) and helped to correlate the data with the electrochemical processes.

The filling and forming of lithium battery cells with electrolytes is a time-consuming process and one of the major cost-drivers in cell manufacturing. A homogeneous electrolyte distribution/wetting of the electrode stacks is critical for the cell performance. NI provides a platform to analyze the filling and wetting processes time resolved and non-destructively. Wedanz et al.[75] studied the isotropic wetting process of electrode stacks of hard case prismatic cells from the outer cell regions toward the cell centers, observing that the wetting speed was reduced closer to the

cell center, and that filling in vacuum can reduce the wetting time by half. Habedank et al.[35] studied the wetting process on three different multilayer pouch cells with different engineered electrodes during *in situ* NR. The different degrees of wetting of the different electrodes, with 30% and 40% porosity and laser structured electrodes, is shown in Figure 4C. After 15 min the electrodes showed varying degrees of wetting, with a better cell wetting observed for the cell with higher porosity, and a significant reduction of wetting time achieved for the laser structured electrodes, thus indicating potential to reduce manufacturing time and costs.

The radiography and tomography studies surveyed above are basically materials attenuation measurements, using polychromatic beams and NI cameras set up in transmission mode. On the other hand, neutron diffraction imaging analyzes the neutrons that are Bragg-scattered by the sample. Different diffraction imaging techniques provide information from crystalline materials on structure transformations, phase compositions, and microstructure properties. Spatial resolutions are modest compared with corresponding X-ray methods, in the range of mm^3 for pencil-beam scans, analyzing the Bragg-scattered beam, and hundreds of microns for Bragg-edge imaging, analyzing the transmitted beam.

Neutron diffraction is well suited to study the structural evolution of cathode and anode materials, for example, to observe the inhomogeneities of the Li phase distributions in a battery cell volume. Senyshyn et al.[61,62] utilized a neutron diffraction N-CT approach to study the evolution of the crystal structures versus SoC and to elucidate the Li distribution in 18650 LIB. They concluded that the determination of Li concentrations by polychromatic N-CT is compromised by beam-hardening artifacts, resulting in pronounced attenuation gradients from the radial outer to the inner cell direction. The use of monochromatic N-CT and laterally resolved neutron diffraction proved a more promising approach and resulted in a more homogeneous Li distribution. Senyshyn et al.[76] used spatially resolved neutron diffraction as a quasi-3D imaging technique, with a gage volume of $2 \times 2 \times 20$ mm^3 to create Li-concentration maps in the graphite anode of a charged 18650 cell by translating and rotating the cell as illustrated in Figure 5A.

Bragg-edge transmission of materials used in LIBs was demonstrated by Butler et al.[63,79], who studied the stepwise evolution of the LiC_6 Bragg edge during dis-/charging in the graphite electrodes of prismatic cells with $LiCoO_2$ (LCO) as the cathode material. Kino et al.[80,81] reported the use of 3D Bragg-edge radiography (2D spatially and energy resolved) for studying crystallographic transitions in the cathodes and anodes of 18650 LIBs at different SoC. Later, Kamiyama et al.[77] utilized the same technique to study the variation of the lithiated graphite structures in a LIB pouch cell. These studies captured the crystallographic phase transitions during dis-/charging of LIBs by a radiographic approach, which yielded thickness-integrated information through the LIB as shown in Figure 5B. The first successful use of 4D Bragg-edge tomography (3D spatially and energy resolved) on ultra-thick directional ice-templated graphite electrodes for LIB cells was reported by Ziesche et al.[78] From a set of energy separated radiographic projections in time-of-flight mode, 4D energy-resolved tomographs were reconstructed for an energy range that included the (hkl) Bragg edges for graphite (002), LiC_{12} (002), and a fully lithiated LiC_6 phase (001). By fitting the Bragg edges on a voxel level, 3D phase maps were obtained showing the phase fractions locally resolved, such as shown for an electrode at ca. 33% SoC as horizontal and vertical orthogonal slices in Figure 5C. The spatial resolution of Bragg-edge imaging is currently limited to >100 μm, given the camera pixel sizes of state-of-the art neutron detectors for time-of-flight experiments.

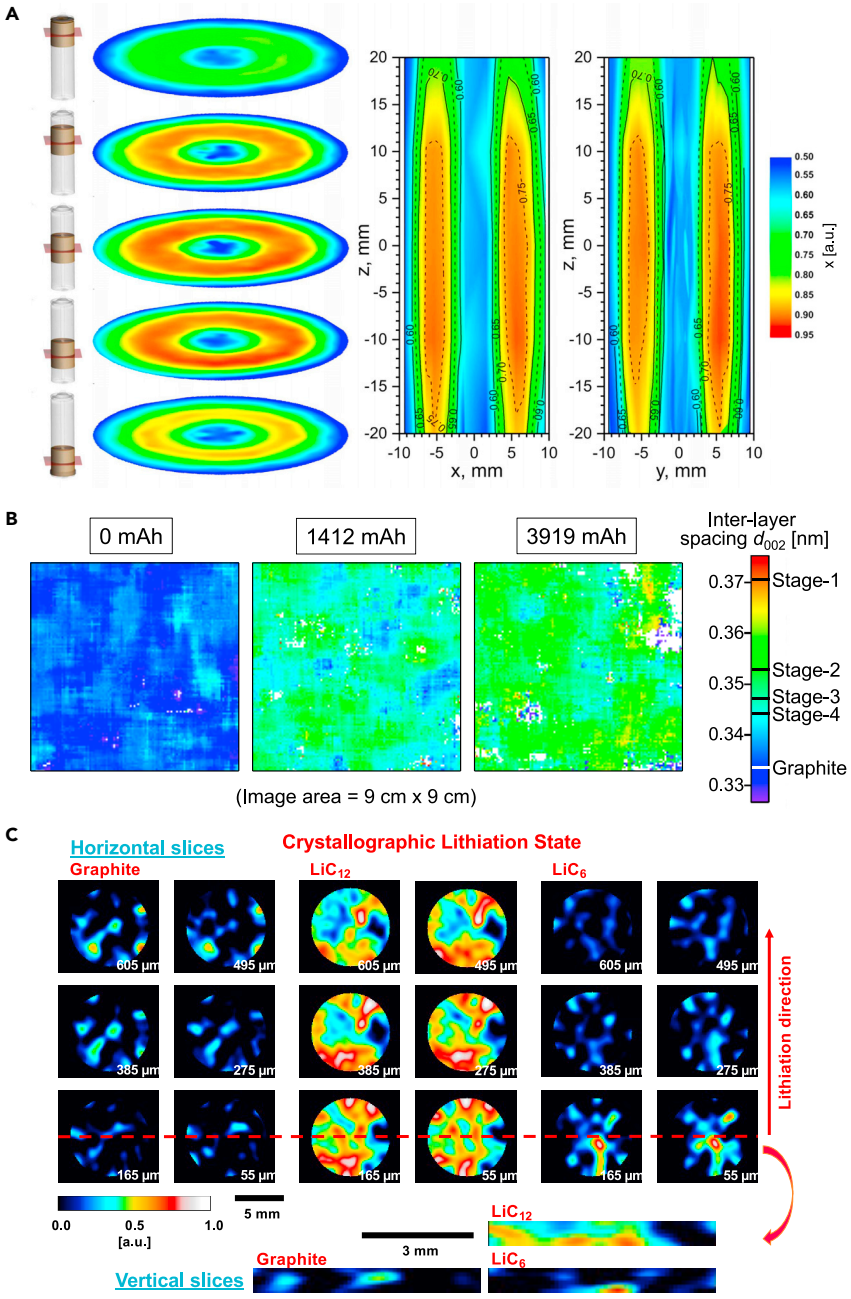

Figure 5. Mapping of the lithium concentration by neutron diffraction imaging techniques

(A) Lithium concentration (x) of Li_xC_6 across horizontal and vertical orthogonal slices of a charged 18650 Li-ion cell by spatially resolved neutron powder diffraction. Reprinted from Senyshyn et al.[76] CC BY 4.0.

(B) 2D mapping of the fractions of (002) graphite and their lithiated stages at different capacities of a multilayer $LiFePO_4$/graphite pouch cell. Reprinted from Kamiyama et al.,[77] with permission from Elsevier CC BY-NC-ND 4.0.

(C) Maps of Bragg-edge heights of graphite, LiC_{12}, and LiC_6 phases for horizontal and vertical orthogonal slices of a directional ice-templated graphite electrode at about 33% SoC. The slices indicate inhomogeneous phase distributions and highest lithiation degree observed close to the lithium-metal counter electrode. Reprinted from Ziesche et al.[78] CC BY 4.0.

PERSPECTIVES

The examples presented in this article demonstrate the significant progress regarding spatial and temporal resolution in NI achieved in the last several years. The further development of the detector technology shows potential for substantial improvements, which would be of great benefit to the majority of applications where the spatial and temporal resolutions need to be traded off against each other for N-CT.

For instance, the upgrade of the most commonly used imaging detector system by the utilization of optical magnification and thin scintillator screens allows a spatial resolution better than 5 μm.[82] A small pixel size and high beam collimation require a high neutron flux to keep exposure times short for *in operando* investigations. For this reason, imaging facility upgrades were started at high-flux, steady-state neutron sources, including the research reactors at the Institut Laue-Langevin (ILL, France) and at NIST (USA). NeXT, a forthcoming instrument at ILL, will provide very intense neutron beams for high resolution and high-speed applications.[82,83] A good source strength is required to resolve the electrode features in the range of a few microns and *in operando* on, for example, a stack of pouch cells in through-plane geometry. While the inspection of sub-micrometer-size features, such as hollow needle-like Li dendrites,[84] will remain beyond the capabilities of NI for the foreseeable future, larger dendritic microstructures[29], or moss like arrangements,[85] with feature sizes from tens of micrometers to the millimeter range, can be examined.

Isotope substitution opens opportunities for contrast variation and noise reduction. Utilizing Li isotopes as contrast agents makes NI a unique technique for dynamic studies of the Li diffusion and intercalation in rechargeable Li cells. A systematic respective substitution of ^{6}Li and ^{7}Li can be exploited to map their distributions *in operando* investigations of real cells in cycling mode. A corresponding approach can be employed for investigating the dynamics in liquid electrolytes by replacing hydrogen with deuterium and for improved visibility of Li and H containing liquid electrolytes.

Besides attenuation imaging, different contrast mechanisms are now utilized in advanced imaging setups. Energy-resolved NI using time-of-flight techniques are under development with the promise of new and unprecedented possibilities. Currently available time-of-flight detector technologies are still limited with regard to pixel and sensor sizes as well count rate capabilities. Moreover, energy-resolving methods are more significantly reliant on high neutron fluxes, which will be available on the forthcoming ODIN instrument at the European Spallation Source (ESS, Sweden)[86], and on the future VENUS and CUPID beamlines at the Spallation Neutron Source (SNS, USA). Current work on the medium-flux IMAT beamline (ISIS, UK) (see Figure 5C),[78] using capabilities that are also available at RADEN (MLF, J-Parc, Japan), demonstrated that the new sources will enable 3D diffraction mapping of different Li stages, for example, LiC_6 and LiC_{12}, potentially in time-lapse mode and with much improved spatial resolution. Such energy-selective multi-spectral imaging[87] will also help to improve data quantification and reduce image artifacts, including beam hardening and scattering distortions of the transmission signal. Direct mapping of the diffraction signals, as demonstrated in Figure 5A, will be possible with much smaller gage volumes on the next-generation strain scanners at pulsed neutron sources. Further, use of neutrons in the thermal, epithermal, and fast neutron energy regimes will benefit studies of large battery types with thicknesses of several centimeters, and potentially allow 2D or 3D mapping of elements and isotopes via neutron resonance analysis using time-of-flight methods.[40]

Progress in hardware is accompanied by the development of advanced image processing tools. The implementation of regularized iterative and neural-network-based reconstruction algorithms, as well as deep learning inspired analysis methods, will help to address some of the drawbacks encountered in NI—such as high-noise and under-sampled data sets—and thus help reduce collection times and improve resolution. This is particularly important for noise-affected multi-spectral imaging. Furthermore, future studies on lithium batteries will endeavor to use neutron and X-rays simultaneously on the same beamline, as the two radiation types are well suited for combinations of imaging/imaging and imaging/diffraction modes on the same samples.

Besides the previously mentioned advantages of NI for Li battery studies, alternative chemistries can be probed, albeit with much-reduced image contrast for carriers in Na-, K-ion, and multivalent metal batteries. If neutron attenuation cross-sections are similar to the bulk components of the battery, the case for NI is much harder to make and high resolution X-ray CT will be more suitable for the majority of systems. However, for Bragg-edge transmission imaging and spatially resolved neutron diffraction, strong absorption is rather unwanted and, thus, diffraction studies will be worth considering for these battery types, to study local microstructure variations and phase transitions inside batteries during cycling.

CONCLUSIONS AND OUTLOOK

In this article, we have reviewed the development of neutron techniques and identified key examples of their application to battery science and engineering from the extant literature. The projected improvements to the suite of neutron techniques, largely enabled by hardware optimization, has been presented. Finally, in this section, we conclude with a perspective on how these tools can be effectively applied to contemporary challenges in battery research.

First, we envisage that the improved accessibility of NI beamlines will facilitate their more widespread adoption; akin to the rapid development and proliferation of X-ray techniques over the past decade, we expect neutron techniques to grow in significance, driven by the unique contrast mechanisms offered. With improving spatial resolution, the increasing ability to reconcile electrode behavior with morphological characteristics will provide insight into the role of micro-scale heterogeneities in determining macroscopic performance, while the improvements in temporal resolution will facilitate routine studies of dynamic cell level phenomena, including *in situ* and *operando* experiments. The current direction of technical advances will support an overall shift from radiographic to tomographic measurements. Generally, we anticipate that the increased throughput offered by developments in both source and detector technology will substantially improve the accessibility of the techniques.

As a non-destructive tool, the extension of 3D NI into the fourth dimension, to evaluate material and device changes over time, and in response to a range of environmental conditions, will also follow the precedents from X-ray imaging. The alternative contrast mechanism not only provides sensitivity to important elemental species, which naturally include metallic Li (and other alkali metals), but also sensitivity to gas generation and liquid electrolyte movement. At the electrode level, key challenges such as dendrite growth will (continue to) be informed by NI, which may be particularly beneficial in solid-state batteries, where the presence of high and low-Z materials—in the form of, for example, ceramic electrolytes and metallic Li,

respectively—can be more readily resolved than with X-ray tools. In tandem with carefully selected isotopic labeling, there is a compelling opportunity to examine the redistribution of active species within an electrode or device. At the cell level, key engineering challenges will also be addressed; for example, those relating to gas generation during dis-/charging or electrolyte drying effects in long term operation. While neutron tools remain much slower than equivalent resolution X-ray imaging, the trajectory for improvements might also see the application of neutron tools for characterization of high-speed events such as thermal runaway. Finally, the introduction of novel techniques, such as Bragg-edge imaging, provide an opportunity to reconcile crystallographic and microstructural information, which can be used to track operation and degradation effects, and identify heterogeneities.

Clearly, neutron techniques are not without limitations. The spatial and temporal resolutions have improved substantially in recent years but are characteristically lower than for X-ray tools. Moreover, the inherent requirement for a neutron source limits the application to large-scale facilities whereas, by contrast, laboratory X-ray generators are commonplace. However, the unique sensitivities and contrast mechanisms of NI techniques offer some compelling benefits and, consequently, NI will become more widely adopted within the pantheon of correlative battery characterization tools.

ACKNOWLEDGMENTS

We would like to acknowledge the Faraday Institution (EP/S003053/1, FIRG013) for supporting research in the Electrochemical Innovation Lab. Financial support from the STFC Batteries Network (ST/R006873/1) is also acknowledged. P.R.S. acknowledges funding from the Royal Academy of Engineering (CiET1718/59). R.F.Z. acknowledges the support of the ISIS Facility Development Studentship.

AUTHOR CONTRIBUTIONS

R.F.Z. and P.R.S. conceived the study. R.F.Z. and all authors wrote, reviewed, and revised the manuscript.

DECLARATION OF INTERESTS

The authors declare no competing interests.

REFERENCES

1. Cheng, X., Liu, H., Yuan, H., Peng, H., Tang, C., Huang, J., and Zhang, Q. (2021). A perspective on sustainable energy materials for lithium batteries. SusMat *1*, 38–50.

2. Han, M.H., Gonzalo, E., Singh, G., and Rojo, T. (2015). A comprehensive review of sodium layered oxides: powerful cathodes for Na-ion batteries. Energy Environ. Sci. *8*, 81–102.

3. Liang, Y., Dong, H., Aurbach, D., and Yao, Y. (2020). Current status and future directions of multivalent metal-ion batteries. Nat. Energy *5*, 646–656.

4. Britton, M.M. (2017). MRI of chemical reactions and processes. Prog. Nucl. Magn. Reson. Spectrosc. *101*, 51–70.

5. Britton, M.M. (2014). Magnetic resonance imaging of electrochemical cells containing bulk metal. ChemPhysChem *15*, 1731–1736.

6. Pecher, O., Carretero-González, J., Griffith, K.J., and Grey, C.P. (2017). Materials' methods: NMR in battery research. Chem. Mater. *29*, 213–242.

7. Krachkovskiy, S.A., Bazak, J.D., Werhun, P., Balcom, B.J., Halalay, I.C., and Goward, G.R. (2016). Visualization of steady-state ionic concentration profiles formed in electrolytes during Li-ion battery operation and determination of mass-transport properties by in situ magnetic resonance imaging. J. Am. Chem. Soc. *138*, 7992–7999.

8. Grey, C.P., and Tarascon, J.M. (2016). Sustainability and in situ monitoring in battery development. Nat. Mater. *16*, 45–56.

9. Chang, H.J., Ilott, A.J., Trease, N.M., Mohammadi, M., Jerschow, A., and Grey, C.P. (2015). Correlating microstructural lithium metal growth with electrolyte salt depletion in lithium batteries using ^{7}Li MRI. J. Am. Chem. Soc. *137*, 15209–15216.

10. Klett, M., Giesecke, M., Nyman, A., Hallberg, F., Lindström, R.W., Lindbergh, G., and Furó, I. (2012). Quantifying mass transport during polarization in a Li-ion battery electrolyte by in situ ^{7}Li NMR imaging. J. Am. Chem. Soc. *134*, 14654–14657.

11. Bray, J.M., Doswell, C.L., Pavlovskaya, G.E., Chen, L., Kishore, B., Au, H., Alptekin, H., Kendrick, E., Titirici, M.M., Meersmann, T., and Britton, M.M. (2020). Operando visualisation of battery chemistry in a sodium-ion battery by 23Na magnetic resonance imaging. Nat. Commun. *11*, 2083.

12. Ilott, A.J., Mohammadi, M., Chang, H.J., Grey, C.P., and Jerschow, A. (2016). Real-time 3D imaging of microstructure growth in battery cells using indirect MRI. Proc. Natl. Acad. Sci. USA *113*, 10779–10784.

13. Goodhew, P.J., Humphreys, J., and Beanland, R. (2000). Electron Microscopy and Analysis, Third Edition (CRC Press).

14. Vernon-Parry, K.D. (2000). Scanning electron microscopy: an introduction. III-Vs Rev. *13*, 40–44.

15. Yang, Q., Li, Q., Liu, Z., Wang, D., Guo, Y., Li, X., Tang, Y., Li, H., Dong, B., and Zhi, C. (2020). Dendrites in Zn-based batteries. Adv. Mater. *32*, e2001854.

16. Foroozan, T., Sharifi-Asl, S., and Shahbazian-Yassar, R. (2020). Mechanistic understanding of Li dendrites growth by in- situ/operando imaging techniques. J. Power Sources *461*, 228135.

17. Rong, G., Zhang, X., Zhao, W., Qiu, Y., Liu, M., Ye, F., Xu, Y., Chen, J., Hou, Y., Li, W., et al. (2017). Liquid-phase electrochemical scanning electron microscopy for in situ investigation of lithium dendrite growth and dissolution. Adv. Mater. *29*, 1606187.

18. Chen, D., Indris, S., Schulz, M., Gamer, B., and Mönig, R. (2011). In situ scanning electron microscopy on lithium-ion battery electrodes using an ionic liquid. J. Power Sources *196*, 6382–6387.

19. Yufit, V., Tariq, F., Eastwood, D.S., Biton, M., Wu, B., Lee, P.D., and Brandon, N.P. (2019). Operando visualization and multi-scale tomography studies of dendrite formation and dissolution in zinc batteries. Joule *3*, 485–502.

20. Finegan, D.P., Darcy, E., Keyser, M., Tjaden, B., Heenan, T.M.M., Jervis, R., Bailey, J.J., Malik, R., Vo, N.T., Magdysyuk, O.V., et al. (2017). Characterising thermal runaway within lithium-ion cells by inducing and monitoring internal short circuits. Energy Environ. Sci. *10*, 1377–1388.

21. Finegan, D.P., Darcy, E., Keyser, M., Tjaden, B., Heenan, T.M.M., Jervis, R., Bailey, J.J., Vo, N.T., Magdysyuk, O.V., Drakopoulos, M., et al. (2018). Identifying the cause of rupture of Li-ion batteries during thermal runaway. Adv. Sci. (Weinh) *5*, 1700369.

22. Daemi, S.R., Tan, C., Vamvakeros, A., Heenan, T.M.M., Finegan, D.P., Di Michiel, M., Beale, A.M., Cookson, J., Petrucco, E., Weaving, J.S., et al. (2020). Exploring cycling induced crystallographic change in NMC with X-ray diffraction computed tomography. Phys. Chem. Chem. Phys. *22*, 17814–17823.

23. Heenan, T.M.M., Wade, A., Tan, C., Parker, J.E., Matras, D., Leach, A.S., Robinson, J.B., Llewellyn, A., Dimitrijevic, A., Jervis, R., et al. (2020). Identifying the origins of microstructural defects such as cracking within Ni-rich NMC811 cathode particles for lithium-ion batteries. Adv. Energy Mater. *10*, 2002655.

24. Chen, C., Wei, Y., Zhao, Z., Zou, Y., and Luo, D. (2019). Investigation of the swelling failure of lithium-ion battery packs at low temperatures using 2D/3D X-ray computed tomography. Electrochim. Acta *305*, 65–71.

25. Larsson, F., Andersson, P., and Mellander, B.E. (2016). Lithium-ion battery aspects on fires in electrified vehicles on the basis of experimental abuse tests. Batteries *2*, 1–13.

26. Robinson, J.B., Finegan, D.P., Heenan, T.M.M., Smith, K., Kendrick, E., Brett, D.J.L., and Shearing, P.R. (2018). Microstructural analysis of the effects of thermal runaway on Li-ion and Na-ion battery electrodes. J. Electrochem. Energy Convers. Storage *15*, 1–9.

27. Yufit, V., Shearing, P., Hamilton, R.W., Lee, P.D., Wu, M., and Brandon, N.P. (2011). Investigation of lithium-ion polymer battery cell failure using X-ray computed tomography. Electrochem. Commun. *13*, 608–610.

28. Yokoshima, T., Mukoyama, D., Maeda, F., Osaka, T., Takazawa, K., Egusa, S., Naoi, S., Ishikura, S., and Yamamoto, K. (2018). Direct observation of internal state of thermal runaway in lithium ion battery during nail-penetration test. J. Power Sources *393*, 67–74.

29. Song, B., Dhiman, I., Carothers, J.C., Veith, G.M., Liu, J., Bilheux, H.Z., and Huq, A. (2019). Dynamic lithium distribution upon dendrite growth and shorting revealed by operando neutron imaging. ACS Energy Lett *4*, 2402–2408.

30. Ziesche, R.F., Arlt, T., Finegan, D.P., Heenan, T.M.M., Tengattini, A., Baum, D., Kardjilov, N., Markötter, H., Manke, I., Kockelmann, W., et al. (2020). 4D imaging of lithium-batteries using correlative neutron and X-ray tomography with a virtual unrolling technique. Nat. Commun. *11*, 777.

31. Ziesche, R.F., Robinson, J.B., Markötter, H., Bradbury, R., Tengattini, A., Lenoir, N., Helfen, L., Kockelmann, W., Kardjilov, N., Manke, I., et al. (2020). Editors' choice—4D neutron and X-ray tomography studies of high energy density primary batteries: Part II. Multi-modal microscopy of LiSOCl 2 cells. J. Electrochem. Soc. *167*, 140509.

32. Ziesche, R.F., Robinson, J.B., Kok, M.D.R., Markötter, H., Kockelmann, W., Kardjilov, N., Manke, I., Brett, D.J.L., and Shearing, P.R. (2020). Editors' choice—4D neutron and X-ray tomography studies of high energy density primary batteries: part I. Dynamic studies of LiSOCl 2 during discharge. J. Electrochem. Soc. *167*, 130545.

33. Goers, D., Holzapfel, M., Scheifele, W., Lehmann, E., Vontobel, P., and Novák, P. (2004). In situ neutron radiography of lithium-ion batteries: the gas evolution on graphite electrodes during the charging. J. Power Sources *130*, 221–226.

34. Starke, B., Seidlmayer, S., Schulz, M., Dinter, A., Revay, Z., Gilles, R., and Pettinger, K.-H. (2017). Gas evolution and capacity fading in $LiFe_xMn_{1-x}PO_4$/graphite cells studied by neutron imaging and neutron induced prompt gamma activation analysis. J. Electrochem. Soc. *164*, A3943–A3948.

35. Habedank, J.B., Günter, F.J., Billot, N., Gilles, R., Neuwirth, T., Reinhart, G., and Zaeh, M.F. (2019). Rapid electrolyte wetting of lithium-ion batteries containing laser structured electrodes: in situ visualization by neutron radiography. Int. J. Adv. Manuf. Technol. *102*, 2769–2778.

36. J. Banhart, ed. (2008). Advanced Tomographic Methods in Materials Research and Engineering (Oxford University Press).

37. Banhart, J., Borbély, A., Dzieciol, K., Garcia-Moreno, F., Manke, I., Kardjilov, N., Kaysser-Pyzalla, A.R., Strobl, M., and Treimer, W. (2010). X-ray and neutron imaging – complementary techniques for materials science and engineering. Int. J. Mater. Res. *101*, 1069–1079.

38. Kak, A.C., and Slaney, M. (1999). Principles of Computerized Tomographic Imaging (IEEE Press).

39. Woracek, R., Santisteban, J., Fedrigo, A., and Strobl, M. (2018). Diffraction in neutron imaging-A review. Nucl. Instrum. Methods Phys. Res. Sect. A Accel. Spectrometers, Detect. Assoc. Equip. *878*, 141–158.

40. Tremsin, A.S., Perrodin, D., Losko, A.S., Vogel, S.C., Shinohara, T., Oikawa, K., Peterson, J.H., Zhang, C., Derby, J.J., Zlokapa, A.M., et al. (2017). In-situ observation of phase separation during growth of $Cs_2LiLaBr_6$:Ce crystals using energy-resolved neutron imaging. Cryst. Growth Des. *17*, 6372–6381.

41. Min, X., Xiao, J., Fang, M., Wang, W., Zhao, Y., Liu, Y., Abdelkader, A.M., Xi, K., Kumar, R.V., and Huang, Z. (2021). Potassium-ion batteries: outlook on present and future technologies. Energy Environ. Sci. *14*, 2186–2243.

42. Kochetov, V., Mühlbauer, M.J., Schökel, A., Fischer, T., Müller, T., Hofmann, M., Staron, P., Lienert, U., Petry, W., and Senyshyn, A. (2021). Powder diffraction computed tomography: a combined synchrotron and neutron study. J. Phys. Condens. Matter *33*, 105901.

43. Kardjilov, N., Manke, I., Woracek, R., Hilger, A., and Banhart, J. (2018). Advances in neutron imaging. Mater. Today *21*, 652–672.

44. Strobl, M., Harti, R.P., Gruenzweig, C., Woracek, R., and Plomp, J. (2017). Small angle scattering in neutron imaging – a review. J. Imaging *3*, 64.

45. Strobl, M., Heimonen, H., Schmidt, S., Sales, M., Kardjilov, N., Hilger, A., Manke, I., Shinohara, T., and Valsecchi, J. (2019). Polarization measurements in neutron imaging. J. Phys. D: Appl. Phys. *52*, 123001.

46. Hussey, D.S., and Jacobson, D.L. (2015). Applications of neutron imaging and future possibilities. Neutron News *26*, 19–22.

47. Kamata, M., Esaka, T., Kodama, N., Fujine, S., Yoneda, K., and Kanda, K. (1996). Application of neutron radiography to visualize the motion of lithium ions in lithium-ion conducting materials. J. Electrochem. Soc. *143*, 1866–1870.

48. Takai, S. (1999). Diffusion coefficient measurement of lithium ion in sintered $Li_{1.33}Ti_{1.67}O_4$ by means of neutron radiography. Solid State Ionics *123*, 165–172.

49. Takai, S., Mandai, T., Kawabata, Y., and Esaka, T. (2005). Diffusion coefficient measurements of $La_{2/3-x}Li_{3x}TiO_3$ using neutron radiography. Solid State Ionics *176*, 2227–2233.

50. Kamata, M., Esaka, T., Fujine, S., Yoneda, K., and Kanda, K. (1997). Lithium batteries: application of neutron radiography. J. Power Sources *68*, 459–462.

51. Strobl, M., Manke, I., Kardjilov, N., Hilger, A., Dawson, M., and Banhart, J. (2009). Advances in neutron radiography and tomography. Journal of Physics D: Applied Physics *42*, 243001.

52. Nie, Z., Ong, S., Hussey, D.S., LaManna, J.M., Jacobson, D.L., and Koenig, G.M. (2020). Probing transport limitations in thick sintered battery electrodes with neutron imaging. Mol. Syst. Des. Eng. *5*, 245–256.

53. Kardjilov, N., Hilger, A., Manke, I., Strobl, M., Treimer, W., and Banhart, J. (2005). Industrial applications at the new cold neutron radiography and tomography facility of the HMI. Nucl. Instrum. Methods Phys. Res. Sect. A Accel. Spectrometers, Detect. Assoc. Equip. *542*, 16–21.

54. Wang, H., Downing, R.G., Dura, J.A., and Hussey, D.S. (2012). In situ neutron techniques for studying lithium ion batteries. In Polymers for Energy Storage and Delivery: Polyelectrolytes for Batteries and Fuel Cells (American Chemical Society), pp. 91–106.

55. Siegel, J.B., Lin, X., Stefanopoulou, A.G., Hussey, D.S., Jacobson, D.L., and Gorsich, D. (2011). Neutron imaging of lithium concentration in LFP pouch cell battery. J. Electrochem. Soc. *158*, A523–A529.

56. Siegel, J.B., Stefanopoulou, A.G., Hagans, P., Ding, Y., and Gorsich, D. (2013). Expansion of lithium ion pouch cell batteries: observations from neutron imaging. J. Electrochem. Soc. *160*, A1031–A1038.

57. Owejan, J.P., Gagliardo, J.J., Harris, S.J., Wang, H., Hussey, D.S., and Jacobson, D.L. (2012). Direct measurement of lithium transport in graphite electrodes using neutrons. Electrochim. Acta *66*, 94–99.

58. Zhou, H., An, K., Allu, S., Pannala, S., Li, J., Bilheux, H.Z., Martha, S.K., and Nanda, J. (2016). Probing multiscale transport and inhomogeneity in a lithium-ion pouch cell using in situ neutron methods. ACS Energy Lett *1*, 981–986.

59. Nie, Z., McCormack, P., Bilheux, H.Z., Bilheux, J.C., Robinson, J.P., Nanda, J., and Koenig, G.M. (2019). Probing lithiation and delithiation of thick sintered lithium-ion battery electrodes with neutron imaging. J. Power Sources *419*, 127–136.

60. Riley, G.V., Hussey, D.S., and Jacobson, D. (2019). In situ neutron imaging of alkaline and lithium batteries. ECS Trans *25*, 75–83.

61. Senyshyn, A., Mühlbauer, M.J., Nikolowski, K., Pirling, T., and Ehrenberg, H. (2012). "In-operando" neutron scattering studies on Li-ion batteries. J. Power Sources *203*, 126–129.

62. Senyshyn, A., Mühlbauer, M.J., Dolotko, O., Hofmann, M., Pirling, T., and Ehrenberg, H. (2014). Spatially resolved in operando neutron scattering studies on Li-ion batteries. J. Power Sources *245*, 678–683.

63. Butler, L.G., Schillinger, B., Ham, K., Dobbins, T.A., Liu, P., and Vajo, J.J. (2011). Neutron imaging of a commercial Li-ion battery during discharge: application of monochromatic imaging and polychromatic dynamic tomography. Nucl. Instrum. Methods Phys. Res. Sect. A Accel. Spectrometers, Detect. Assoc. Equip. *651*, 320–328.

64. Zhang, Y., Chandran, K.S.R., and Bilheux, H.Z. (2018). Imaging of the Li spatial distribution within V_2O_5 cathode in a coin cell by neutron computed tomography. J. Power Sources *376*, 125–130.

65. Nanda, J., Bilheux, H., Voisin, S., Veith, G.M., Archibald, R., Walker, L., Allu, S., Dudney, N.J., and Pannala, S. (2012). Anomalous discharge product distribution in lithium-air cathodes. J. Phys. Chem. C *116*, 8401–8408.

66. Sun, F., Markötter, H., Manke, I., Hilger, A., Alrwashdeh, S.S., Kardjilov, N., and Banhart, J. (2017). Complementary X-ray and neutron radiography study of the initial lithiation process in lithium-ion batteries containing silicon electrodes. Appl. Surf. Sci. *399*, 359–366.

67. Sun, F., Gao, R., Zhou, D., Osenberg, M., Dong, K., Kardjilov, N., Hilger, A., Markötter, H., Bieker, P.M., Liu, X., and Manke, I. (2019). Revealing hidden facts of Li anode in cycled lithium–oxygen batteries through X-ray and neutron tomography. ACS Energy Lett *4*, 306–316.

68. LaManna, J.M., Hussey, D.S., Baltic, E.M., and Jacobson, D.L. (2017). Improving material identification by combining x-ray and neutron tomography. Proc. SPIE *1039104*, 1–7.

69. LaManna, J.M., Hussey, D.S., DiStefano, V.H., Baltic, E., and Jacobson, D.L. (2020). NIST NeXT: a system for truly simultaneous neutron and X-ray tomography. Proceedings Volume 11494, Hard X-Ray, Gamma-Ray, and Neutron Detector Physics XXII, p. 114940P.

70. Kaestner, A., Münch, B., Trtik, P., and Butler, L. (2011). Spatiotemporal computed tomography of dynamic processes. Opt. Eng. *50*, 123201.

71. Kohler, T. (2004). A projection access scheme for iterative reconstruction based on the golden section. IEEE Symposium Conference Record Nuclear Science, 3961–3965.

72. Lanz, M., Lehmann, E., Imhof, R., Exnar, I., and Novák, P. (2001). In situ neutron radiography of lithium-ion batteries during charge/discharge cycling. J. Power Sources *101*, 177–181.

73. Michalak, B., Sommer, H., Mannes, D., Kaestner, A., Brezesinski, T., and Janek, J. (2015). Gas evolution in operating lithium-ion batteries studied in situ by neutron imaging. Sci. Rep. *5*, 15627.

74. Michalak, B., Berkes, B.B., Sommer, H., Bergfeldt, T., Brezesinski, T., and Janek, J. (2016). Gas evolution in $LiNi_{0.5}Mn_{1.5}O_4$/graphite cells studied in operando by a combination of differential electrochemical mass spectrometry, neutron imaging, and pressure measurements. Anal. Chem. *88*, 2877–2883.

75. Weydanz, W.J., Reisenweber, H., Gottschalk, A., Schulz, M., Knoche, T., Reinhart, G., Masuch, M., Franke, J., and Gilles, R. (2018). Visualization of electrolyte filling process and influence of vacuum during filling for hard case prismatic lithium ion cells by neutron imaging to optimize the production process. J. Power Sources *380*, 126–134.

76. Senyshyn, A., Mühlbauer, M.J., Dolotko, O., Hofmann, M., and Ehrenberg, H. (2015). Homogeneity of lithium distribution in cylinder-type Li-ion batteries. Sci. Rep. *5*, 18380.

77. Kamiyama, T., Narita, Y., Sato, H., Ohnuma, M., and Kiyanagi, Y. (2017). Structural change of carbon anode in a lithium-ion battery product associated with charging process observed by neutron transmission bragg-edge imaging. Phys. Procedia *88*, 27–33.

78. Ziesche, R.F., Tremsin, A.S., Huang, C., Tan, C., Grant, P.S., Storm, M., Brett, D.J.L., Shearing, P.R., and Kockelmann, W. (2020). 4D Bragg edge tomography of directional ice templated graphite electrodes. J. Imaging *6*, 136.

79. Butler, L.G., Lehmann, E.H., and Schillinger, B. (2013). Neutron radiography, tomography, and diffraction of commercial lithium-ion polymer batteries. Phys. Procedia *43*, 331–336.

80. Kino, K., Yonemura, M., Kiyanagi, Y., Ishikawa, Y., Parker, J.D., Tanimori, T., and Kamiyama, T. (2015). First imaging experiment of a lithium ion battery by a pulsed neutron beam at J-PARC/MLF/BL09. Phys. Procedia *69*, 612–618.

81. Kino, K., Yonemura, M., Ishikawa, Y., and Kamiyama, T. (2016). Two-dimensional imaging of charge/discharge by Bragg edge analysis of electrode materials for pulsed neutron-beam transmission spectra of a Li-ion battery. Solid State Ionics *288*, 257–261.

82. Tengattini, A., Lenoir, N., Andò, E., Giroud, B., Atkins, D., Beaucour, J., and Viggiani, G. (2020). NeXT-Grenoble, the neutron and X-ray tomograph in Grenoble. Nucl. Instrum. Methods Phys. Res. Sect. A Accel. Spectrometers, Detect. Assoc. Equip. *968*, 1–11.

83. Tötzke, C., Kardjilov, N., Lenoir, N., Manke, I., Oswald, S.E., and Tengattini, A. (2019). What comes NeXT ? – high-speed neutron tomography at ILL. Opt. Express *27*, 28640–28648.

84. Golozar, M., Hovington, P., Paolella, A., Bessette, S., Lagacé, M., Bouchard, P., Demers, H., Gauvin, R., and Zaghib, K. (2018). In situ scanning electron microscopy detection of carbide nature of dendrites in Li-polymer batteries. Nano Lett *18*, 7583–7589.

85. Chang, H.J., Trease, N.M., Ilott, A.J., Zeng, D., Du, L.S., Jerschow, A., and Grey, C.P. (2015). Investigating Li microstructure formation on Li anodes for lithium batteries by in situ $^6Li/^7Li$ NMR and SEM. J. Phys. Chem. C *119*, 16443–16451.

86. Andersen, K.H., Argyriou, D.N., Jackson, A.J., Houston, J., Henry, P.F., Deen, P.P., Toft-Petersen, R., Beran, P., Strobl, M., Arnold, T., et al. (2020). The instrument suite of the European Spallation Source. Nucl. Instrum. Methods Phys. Res. Sect. A Accel. Spectrometers, Detect. Assoc. Equip. *957*, 163402.

87. Tran, K.V., Woracek, R., Kardjilov, N., Markötter, H., Hilger, A., Kockelmann, W., Kelleher, J., Puplampu, S.B., Penumadu, D., Tremsin, A.S., et al. (2021). Spectral neutron tomography. Mater. Today Adv. *9*, 100132.